The principle of minimal episteric distortion of the water matrix and its role in protein folding

Ariel Fernández [1,2,3]

[1] *Instituto Argentino de Matemática, CONICET (National Research Council), Saavedra 15, Buenos Aires 1083, Argentina*

[2] *Collegium Basilea, Institute for Advanced Study, Hochstrasse 51, CH 4053 Basel, Switzerland*

[3] *Ariel Fernández Innovation, Pharmaceutical Consultancy, Avenida del Libertador 1092, Piso 1, Buenos Aires 1112, Argentina*

Phone: 54 11 4954 6781; Fax: 54 11 4954 6782; E-mail: ariel@afinnovation.com

A significant episteric ("around a solid") distortion of the hydrogen-bond structure of water is promoted by solutes with nanoscale surface detail and physico-chemical complexity, such as soluble natural proteins. These structural distortions defy analysis because the discrete nature of the solvent at the interface is not upheld by the continuous laws of electrostatics. This work derives and validates an electrostatic equation that governs the episteric distortions of the hydrogen-bond matrix. The equation correlates distortions from bulk-like structural patterns with anomalous polarization components that do not align with the electrostatic field of the solute. The result implies that the interfacial energy stored in the orthogonal polarization correlates with the distortion of the water hydrogen-bond network. The result is validated vis-à-vis experimental data on protein interfacial thermodynamics and is interpreted in terms of the interaction energy between the electrostatic field of the solute and the dipole moment induced by the anomalous

polarization of interfacial water. Finally, we consider solutes capable of changing their interface through conformational transitions and introduce a principle of minimal episteric distortion (MED) of the water matrix. We assess the importance of the MED principle in the context of protein folding, concluding that the native fold may be identified topologically with the conformation that minimizes the interfacial tension or disruption of the water matrix.

PACS numbers: 61.20.-p, 97.10.Ed

I. INTRODUCTION

The multi-scale structure of water in the condensed phases of biological relevance remains a source of controversy.[1,2] In bulk water, the controversy arises and has been partly fuelled by the discovery of structural distortions in the fluctuating tetrahedral hydrogen-bond lattice due to asymmetric electron density in liquid water, detectable by X-ray absorption at effective Bragg spacing $d<0.96$Å (or $Q>6.5$Å^{-1}, $Q=2\pi/d$ is the momentum transfer).[1] On the other hand, the long-range tetrahedral hydrogen-bond network signatures are clearly present in the X-ray scattering intensity and structure factor data for $d>0.96$Å.[2] Thus, at nano-meter scales we may assume that the structure of water with its resilient tetrahedral lattice of intermolecular hydrogen bonds is largely responsible for its significant dielectric properties. As it is known, this resilience to the polarization induced by an external electrostatic field generated by a charge separation is reflected in the large permittivity coefficient of water.

Provided tetrahedral coordination possibilities are preserved as in bulk-like environments, polarization is believed to align with electrostatic fields determined by fixed charges, as first proposed by Peter Debye.[3-6] There are indications that this “Debye

ansatz" [7] may break down under confinement of water molecules in regions of nanoscale dimensions.[4] The breakdown is attributed to the fact that the bulk-like floppy tetrahedral lattice has been distorted to a point where water is effectively deprived of hydrogen-bond partnerships[6] and tends to preserve its interfacial hydrogen-bond pattern in spite of the field-aligning torque imposed by the electrostatic field.[4] For instance, the complexities of dielectric properties at biological heterogeneous interfaces [8-10] bespeak of a spatial scale where the behavior of water dipoles cannot be accounted for through linear polarization relations.[5,11-13] The nanoscale structure of water must be inevitably incorporated into the electrostatic description of "*episteric*" fields at interfaces that confine the solvent to discrete levels.[5,14] By *episteric* we mean surrounding a solute particle with a defined interface and charge distribution, such as a soluble protein.

The laws of dielectric response are inherently continuous,[7] at odds with the discrete structural distortions of water that promote anomalous polarization under nanoscale confinement. To exploit the mathematical apparatus of electrostatics, we face the conundrum of having to adopt continuous –actually differentiable- descriptive functions for water that are inadequate at scales where its discrete hydrogen-bond coordination becomes significant. To reconcile these conflictive aspects, we introduce a local indicator of time-averaged hydrogen-bonding patterns for water molecules at spatial locations. Specifically, we introduce a scalar field $g=g(\mathbf{r})$ indicating the time-averaged number of hydrogen bonds of a water molecule computed while its barycenter is contained within a sphere of radius r=4Å centered at position $\mathbf{r}$ and during a timespan τ=1ns. The (r, τ)-parametrization of this scalar field has been calibrated empirically (Supplemental Material), so that the choices r=4Å, τ=1ns represent minimal values guaranteeing second-

order differentiability for g. This level of smoothness is required to introduce a nanoscale dielectric equation. The g-function indicates in a coarse grained way the number of interactions of a water molecule within a neighborhood of each point in space, remaining informative at ~1nm levels. Yet, as previous results suggest,[1] g would be a poor descriptor of water structure for sub-angstrom effective Bragg spacing. By definition, $g=g(\mathbf{r})$ represents also an average over all water molecules visiting the sphere within the 1ns-timespan. The hydrogen bonds counted involve neighboring water molecules and polar groups.

The episteric polarization $\mathbf{P}=\mathbf{P}(\mathbf{r})$ of water is expected to depart from the linear dielectric relation $\mathbf{P}=(\varepsilon-\varepsilon_o)\mathbf{E}$ ($\mathbf{E}$=internal electrostatic field, ε_o=vacuum permittivity, ε=effective local permittivity) wherever $g(\mathbf{r})$ signals a distortion ($g<4$) from the tetrahedral coordination pattern representative of bulk water ($g=4$).[2] Specifically, we have shown that departures from bulk-like coordination introduce a significant component of polarization, $\mathbf{P}^{\#}$, orthogonal to $\mathbf{E}$.[4] This "anomalous" polarization is the resultant of the partial hindrance in the alignment of water dipoles with the field $\mathbf{E}$ due to nanoscale confinement (Fig. 1). Thus, orthogonal polarization is promoted by a nanoscale interfacial topography precluding complete cancellation of the partial charges distributed tetrahedrically on the molecular orbitals of water.

The departure from the "linear dielectrics" picture is rigorously characterized in terms of a partial differential equation valid at nanoscales. The equation governs the episteric distortions in the water hydrogen-bond matrix and reconciles the inherently discrete nature of the water matrix with the continuous laws of electrostatics by revealing a

correlation between the energies stored in distortions of water structure and in the orthogonal polarization.

Since there is a significant free-energy cost associated with the episteric distortion of the water matrix, it is expected that solutes such as proteins, capable of changing their interface with water through internal conformational change would do so subject to a principle of minimal episteric distortion (MED). This is indeed the case as shown in section V. Our results uphold the MED principle as a determinant of the protein folding process. These results lead us to conclude that the native fold is the conformation that minimizes the interfacial tension or, equivalently, entail the minimum disruption of the water structure.

II. DIELECTRICS UNDER NANOSCALE CONFINEMENT

To treat dielectrics under nanoscale confinement, we adopt as starting point the Poisson equation $\nabla.(\varepsilon_o \mathbf{E})=\rho+\Gamma$ for the field $\mathbf{E}$, where $\rho = \rho(\mathbf{r})$ is the fixed charge distribution, and $\Gamma = \Gamma(\mathbf{r}) = -\nabla.\mathbf{P}$ is the net charge distribution induced by polarization. In our context, polarization is not only due to dipole alignment along the **E**-field lines but also a resultant of the nanoscale water structure. Thus, the Poisson equation reads:

$$\nabla.(\varepsilon_o \mathbf{E} + \mathbf{P}) = \nabla.(\varepsilon_o \mathbf{E} + \mathbf{P}^{\|} + \mathbf{P}^{\#}) = \rho, \qquad (1)$$

where, without loss of generality, $\mathbf{P}$ is decomposed into a field-aligned component $\mathbf{P}^{\|}=(\mathbf{P}.\mathbf{e})\mathbf{e}$ ($\mathbf{e}=\mathbf{E}/\|\mathbf{E}\|$) and a component $\mathbf{P}^{\#}$, orthogonal to $\mathbf{E}$. Accordingly we define aligned ($\Gamma^{\|}$) and orthogonal ($\Gamma^{\#}$) induced charges:

$$-\nabla.\mathbf{P}^{\|} = \Gamma^{\|} \text{ and } -\nabla.\mathbf{P}^{\#}=\Gamma^{\#}, \text{ with } \Gamma^{\|}+\Gamma^{\#} =\Gamma \qquad (2)$$

From Eq. 1 we rigorously obtain:

$$\nabla.(\mathbf{P}^{\#}) = \rho - \nabla.[\varepsilon_o\mathbf{E} + \mathbf{P}^{||}] \quad (3)$$

Since departures from bulk water structure (spatially measured by $\nabla g \neq 0$) induce orthogonal polarization, we adopt the ansatz $\mathbf{P}^{\#} \propto \nabla g$, or $\mathbf{P}^{\#} = \xi\nabla g$,[4] where $\xi = (\lambda\varepsilon_o)^{1/2}$ and the parameter λ is obtained by estimation of the interfacial free energy of a nonpolar sphere with radius θ and contrasting in the macroscopic limit the result with the elastic integral $\int \frac{1}{2}||\nabla g||^2 d\mathbf{r}$. The elastic integrand $\frac{1}{2}||\nabla g||^2$ accounts for tension-generating reductions in water coordination ($||\nabla g|| > 0$) and vanishes everywhere except at the solute-water interface. The comparison is valid since interfacial tension is related to the distortion of the tetrahedral coordination structure of bulk water. In the macroscopic limit, where $\theta >> 1$nm, we get $\lambda = 9.0\text{mJ/m} = \lim [\gamma(4\pi\theta^2)/\int \frac{1}{2}||\nabla g||^2 d\mathbf{r}]$, where $\gamma = 72\text{mJ/m}^2$ is the macroscopic surface tension of water at 298K.

Given the assumption $\mathbf{P}^{\#} = \xi\nabla g$, Eq. 3 can be written as a relation between the curvature $\nabla^2 g$ and the term $-\Gamma^{\#} = -\Gamma + \Gamma^{||} = -\Gamma - \nabla.\mathbf{P}^{||} = \rho - \nabla.[\varepsilon_o\mathbf{E} + \mathbf{P}^{||}]$ measuring the departure from the linear dielectrics:

$$\xi\nabla^2 g = -\Gamma^{\#} \quad (4)$$

Eq. 4 incorporates the nanoscale structure of water within an electrostatic relation, revealing that the curvature of the scalar field g is a measure of the departure from linear dielectrics. Eq. 4 is not fully derived from first principles, as supporting Eqs. 1-3 are, but hinges on the assumption that distortions of bulk water structure (measured by $\nabla g \neq 0$) promote orthogonal polarization. This assumption is justified *a posteriori*, as shown in Fig. 2.

To obtain a partial differential equation for a structure-related variable ϕ we first note that at each position **r**, the dimensionless $\Gamma^{\#}/\Gamma$ measures the local deviation from a Debye scenario where polarization fully aligns with **E**, and so does the structure-related variable ϕ=4-g, where ϕ=0 indicates no deviation, as in bulk-like water structure. Thus, we expect that a relation of the form: $\Gamma^{\#}/\Gamma = c\phi$ must hold, where c is a proportionality constant. This relation is indeed valid with c=0.191 as shown in Fig. 2a. The quotient $\Gamma^{\#}/\Gamma$ is computed at protein/water interfaces as a time average over a 10ns-period beyond equilibration of the protein structure with the solvent. Thus, the episteric polarization **P**=**P(r)** for 9 soluble natural proteins with structures reported in the Protein Data Bank (PDB, Supplementary Material, Table S1 [19]) is computed along thermalization molecular dynamics trajectories (Supplementary Material).[19] Each 10ns-trajectory is generated using as starting point the equilibrated structural coordinates that result after thermalization of the PDB-reported structure immersed in a pre-equilibrated solvent bath. Simulations are performed within an isobaric/isothermal ensemble (1atm, 298K). A total of 100 interfacial solvent configurations, one per 100ps along a 10ns-thermalization trajectory, are used to compute the episteric polarization quotient $\Gamma^{\#}/\Gamma$ as a time average using the relation

$$\Gamma^{\#}/\Gamma = \{\rho - \mathbf{\nabla}.[\varepsilon_o \mathbf{E} + \mathbf{P}^{\|}]\}/\{\rho - \mathbf{\nabla}.[\varepsilon_o \mathbf{E}]\} = 1 - \{\mathbf{\nabla}.\mathbf{P}^{\|}\}/\{\rho - \mathbf{\nabla}.[\varepsilon_o \mathbf{E}]\} \qquad (5)$$

To this end, we recorded charge distribution $\rho(\mathbf{r}, t)$, internal field $\mathbf{E}(\mathbf{r}, t)$ and polarization $\mathbf{P}(\mathbf{r}, t)$ from the 100 snapshots that partition the 10ns period in identical intervals.

The structure/solvent system is considered equilibrated at time t_o if the RMSD of backbone atomic coordinates averaged over randomly chosen pairs of chain conformations within a time interval $[t_o, t_o + \tau]$ ($\tau \approx$1ns) is less than 1Å. For all 9 proteins

in this study, this criterion was fulfilled for t_o=500ps. Solvent and side-chain conformations continue to vary significantly (i.e. RMSD>2.25Å) on the 1ns timescale.

By introducing the relation $\Gamma^{\#}=c\Gamma\phi$, and defining the constant $k=c/\xi$, Eq. (4) becomes a linear homogeneous differential equation in ϕ of the Schrödinger type:

$$-\nabla^2\phi + k\Gamma\phi = 0 \qquad (6)$$

The boundary conditions are described in Fig. 1 and are determined by the water-smeared envelope $\partial\Omega$ of the solute-protein interface. Thus, ϕ=4 (no water) in the "core" volume Ω_0 at distance d=2r=8Å from each point on $\partial\Omega$, while ϕ=0 for points at distance larger than 3d=24Å from $\partial\Omega$. The latter condition holds since 3d >> 4 water layers (~13Å) from the interface and hence in this region, water structure is assumed to have recovered its bulk-like tetrahedral pattern.

The behavior of $\phi=\phi(x)$ relative to the distance x to an interface is indicative of the propagation in space of the distortion of the water structure and is shown in Fig. 2b. The results were obtained by numerical integration of Eq. 6 for structural perturbations generated by confinement of water at the interface. To eliminate confounding factors, the interface was assumed nonpolar and physico-chemically featureless, consisting of a concave region of fixed curvature radius θ, capable of partially confining water molecules, with x=0 representing the center of curvature of the surface. The flat surface represents the macroscopic limit θ>>1nm, and the interfacial ϕ-value is expectedly close to 1 (g~3), as revealed by the grey plot in Fig. 2b. Other perturbations were obtained for θ=3Å (thin black plot), and θ=2.5Å (thick black plot), generating $\phi(0)$=2.01 and $\phi(0)$=2.3, respectively. In all cases, the matrix distortion decays to zero for x>11Å (less than 4 water layers). No water molecule enters the cavity if doing so implies that the

molecule retains on average less than 1.6 hydrogen bonds, making the range $\phi(0)>2.4$, or $\theta<2.37$Å, a forbidden region in real terms.

Eq. (6) is the central result of this work and governs the interplay between episteric polarization, subsumed in Γ, and the nanoscale structure of interfacial water described by ϕ. The estimation of $k=c/\xi$ stems from molecular dynamics computations (Fig. 2). The result follows from the rigorous electrostatic equation 3, combined with the empirical assumption that structural distortions promote orthogonal polarization. This tenet is justified computationally (Fig. 2) by establishing the linear correlation between the proportion of orthogonal polarization $\Gamma^{\#}/\Gamma$ and the structural distortions measured by the parameter ϕ.

To validate Eq. 6, we first compute the energy increment ΔU_ϕ associated with spanning a protein/water interface. This energy is in fact an elastic contribution stored in the distortion of water structure,[3] with $\nabla\phi(\mathbf{r})$ measuring the local structural distortion at position $\mathbf{r}$, and an elastic integrand $(1/2)\lambda\|\nabla\phi(\mathbf{r})\|^2 d\mathbf{r}$ (λ = 9.0mJ/m [4]) quantifying the energetic contribution of spanning a differential region $d\mathbf{r}$ centered at point $\mathbf{r}$.[3] Then, using Gauss' divergence theorem (Supplementary Material)[19] we obtain:

$$\Delta U_\phi = (1/2)\lambda \int \|\nabla\phi\|^2 d\mathbf{r} = -(1/2)\lambda \int \phi \nabla^2\phi \, d\mathbf{r} \qquad (7)$$

Using Eq. 6, we can substitute the integrand $\phi\nabla^2\phi$ in the r. h. s. of Eq. 7 for the term $k\Gamma\phi^2$, obtaining the alternative expression for the interfacial elastic energy:

$$\Delta U_\phi = -(1/2)\, c\, (\lambda/\varepsilon_o)^{1/2} \int \Gamma\phi^2 d\mathbf{r} \qquad (8)$$

Since $\Delta U_\phi = (1/2)\lambda \int \|\nabla\phi\|^2 d\mathbf{r} \geq 0$ ($\lambda>0$, while $\|\nabla\phi\|^2 \geq 0$), the r.h.s of Eq. 8 is a positive term, and thus Eqs. 7,8 imply the general result:

$$\int \Gamma\phi^2 d\mathbf{r} \leq 0, \quad (9)$$

corroborated in all study cases (Fig. 3a). Since $\Gamma=-\nabla.\mathbf{P}$ is the net charge induced by polarization, Eq. 9 implies that *water molecules tend to organize leaving negative charges uncompensated ($\Gamma<0$) when deprived of hydrogen bonding opportunities* ($\phi>0$).

III. MODEL VALIDATION

The interfacial energy stored in the anomalous polarization or, equivalently, in the distortion of water structure, is more readily evaluated using Eq. 8. In this section this result is contrasted against thermodynamic data on the spanning of aqueous interfaces with nanoscale detail. Thus, a suitable testing ground for Eq. 6 is provided by the aqueous interfaces for soluble monomeric proteins with a stable fold characterized by structural and thermodynamic information (Supplementary Material, Table S1).[19] To compare with thermodynamic data we introduce the entropic cost of solvent confinement at the interface $\Delta S_\phi = k_B ln[\Pi_j g_j/4]$, where k_B = Boltzmann constant, g_j= time averaged number of hydrogen bonds for the jth- water molecule, and the dummy index j labels molecules within 3d=24Å from the solvent-smeared envelope $\partial\Omega$ of the protein (Fig. 1). Note that $-T\Delta S_\phi \geq 0$ and reinforces the trend determined by ΔU_ϕ. The reversible work, $\Delta G_\phi = \Delta U_\phi - T\Delta S_\phi \geq 0$, performed on the system to span the protein-water interface is destabilizing of the native fold, thus facilitating thermal denaturation, and hence should anticorrelate with the free energy change for protein denaturation, as it is the case (Fig. 3a).

To assess the folding-destabilizing effects of spanning the interface of the folded protein, we examined the same soluble monomeric proteins used to generate the data in Fig. 2 (Supplementary Material).[19] In thermodynamic terms, protein denaturation is

facilitated proportionally to the reversible work required to span the interface, attesting to the folding-destabilizing effect of interfacial tension arising from the structural distortion of surrounding water. Thus, the computed reversible work ΔG_ϕ for creating the interface measures the extent to which the "protein structure is at odds with the structure of surrounding water" since it quantifies the distortion of water structure around the protein. The tight anticorrelation between ΔG_ϕ and the stability of the protein structure provides experimental support to the underlying Eq. 6 since it reveals that protein destabilization is commensurate with the thermodynamic cost of creating its interface with water, computed using Eq. 8. This observation prompts us to formulate the principle of minimal episteric distortion (MED) that should govern conformational changes in the solute that generate concomitant changes in the interface. The validity of the MED principle in the context of protein folding is upheld in section V.

IV. MODEL INTERPRETATION

An energetic measure of the extent of anomalous polarization relative to the field **E** is provided by the interaction between **E** and the dipole moment $\boldsymbol{\mu}_{\mathbf{P}^\#}$ induced by $\mathbf{P}^\#$, this energetic indicator, denoted $W^\#$, is given by

$$W^\# = W(\mathbf{E}, \mathbf{P}^\#) = -\int \mathbf{E}(\mathbf{r}).\, d\boldsymbol{\mu}_{\mathbf{P}^\#}(\mathbf{r}) = \int\int \mathbf{E}(\mathbf{r}).[(\mathbf{r}'-\mathbf{r})\nabla.\mathbf{P}^\#(\mathbf{r}')]\, d\mathbf{r}'d\mathbf{r} \qquad (10)$$

To obtain this result, we took into account that the differential dipole moment $\boldsymbol{\mu}_{\mathbf{P}^\#}(\mathbf{r})$ induced by $\mathbf{P}^\#$ at position **r** is

$$\boldsymbol{\mu}_{\mathbf{P}^\#}(\mathbf{r}) = -\int [(\mathbf{r}'-\mathbf{r})\nabla.\mathbf{P}^\#(\mathbf{r}')]\, d\mathbf{r}'. \qquad (11)$$

Eqs. 10, 11 follow directly from the laws of electrostatics governing the interaction of a field and a dipole induced by another field.

Combining Eq. 10 with Eq. 6 and using the previous relation $\mathbf{P}^{\#} = \xi\nabla g = -\xi\nabla\phi$, we obtain:

$$W^{\#} = c \int \int \mathbf{E(r).[(r-r')]}\Gamma\mathbf{(r')}\phi\mathbf{(r')}d\mathbf{r}'d\mathbf{r} \quad (12)$$

Thus, Eq. 12 enables the computation of the interaction energy between the internal field and the anomalous non-aligned dipole moment of interfacial water. On the other hand, the Debye interaction energy is given by

$$W^{\|} = W(\mathbf{E}, \mathbf{P}^{\|}) = -\int \mathbf{E(r).}\, d\boldsymbol{\mu}_{\mathbf{P}\|}\mathbf{(r)} = \int \int \mathbf{E(r).[(r'-r)}\nabla\mathbf{.P}^{\|}\mathbf{(r')]}\, d\mathbf{r}'d\mathbf{r} =$$

$$= -\int \int \mathbf{E(r).[(r'-r)]}\, \Gamma^{\|}\mathbf{(r')}\, d\mathbf{r}'d\mathbf{r} \quad (13)$$

Since the interfacial energy has been shown in Eq. 8 to be stored in the orthogonal anomalous polarization, it is expected that $W^{\#}$ would be tightly correlated with ΔU_{ϕ}, in contrast with the Debye energy counterpart $W^{\|}$. This is indeed the case, as shown in Fig. 3b, where the data has been normalized by solvent exposed surface area (SASA) to enable comparison of energetic data across the 9 proteins studied (Table S1, Supplementary Material).[19] These results provide an interpretation of the interfacial tension as an estimator of the breakdown of the Debye ansatz.

V. THE PRINCIPLE OF MINIMAL EPISTERIC DISTORTION AND ITS RELEVANCE IN STEERING THE PROTEIN FOLDING PROCESS

As revealed in Fig. 3, the episteric distortion of the water matrix entails a significant thermodynamic cost associated with spanning the solute-water interface. Thus, we expect that solutes capable of changing their interface through internal conformational change would do so subject to a principle of minimal episteric distortion (MED). The results in

this section uphold this view, suggesting that the MED principle is a decisive factor steering the protein folding process.

To probe this hypothesis, we run folding trajectories covering physically relevant timescales guided by "coarse moves" in the backbone (Φ, Ψ) dihedral torsions of the protein chain.[15,16] Each coarse move is defined by transitions between basins of attraction (R-basins) in the Ramachandran (Φ, Ψ)-map for each residue along the chain. A Ramachandran map plots the internal energy of a residue versus the free dihedral backbone angles, and the R-basins are the allowed regions in (Φ, Ψ)-space.[15-16] Thus, each coarse move represents a transition of the over-all topology of the protein chain where the string of (Φ, Ψ)-values is described in a coarse grained manner by identifying the R-basins where the torsional values lie. Since each residue is assigned an R-basin after a coarse move, the topology of the chain is in effect an ensemble of detailed conformations, with each conformation generated by selecting individual (Φ, Ψ)-coordinates within the assigned R-basins. After each coarse move, the system is allowed to equilibrate with the solvent for 1ns with backbone torsional angles constrained to remain within the pre-assigned R-basins. The equilibration is performed in accord with the protocol described in Supplementary Material[19] subject to the constraints in (Φ, Ψ)-coordinates specified above. Other internal coordinates including side-chain torsional degrees of freedom and solvent coordinates are allowed to vary freely during equilibration.

To reach timescales of relevance to the folding process (>10μs)[15,16], the folding process is steered by the coarse-grained stochastic process. The latter is defined in the time range [t, t+τ] (τ =1ns=fixed time step) by the probability p(t) of the transition $\mathbf{B}(t) \rightarrow \mathbf{B}(t+\tau)$ for

each vector of assigned R-basins $\mathbf{B}(t)=(B_1(t), B_2(t) \ldots, B_N(t))$ representing the topology of the chain at time t, where N is the chain length and the dummy index denotes residue contour position. The initial coarse state of the chain, $\mathbf{B}(0)$, is obtained by random assignment of R-basins for individual residues. All thermodynamic quantities (ΔG, ΔH, ΔS, ΔG_ϕ, ΔS_ϕ, etc.) are computed relative to the initial random coil ensemble or coarse state $\mathbf{B}(0)$. The transition probability p(t) is dependent on the overall free-energy difference between the two consecutive coarse states: $\Delta\Delta G(t)= \Delta\Delta H(t)-T\Delta\Delta S(t)=\Delta G(\mathbf{B}(t+\tau))-\Delta G(\mathbf{B}(t))$, where the enthalpy contribution $\Delta\Delta H(t)$ is in effect determined in the NPT ensemble[19] by the energy difference between the two equilibrated conformations belonging to topologies $\mathbf{B}(t+\tau)$ and $\mathbf{B}(t)$, respectively. The entropy difference $\Delta\Delta S(t)$ is obtained from the Boltzmann formula: $\Delta\Delta S(t)=k_B ln[Z(\mathbf{B}(t+\tau))/Z(\mathbf{B}(t))]$, where k_B is the Boltzmann constant and $Z(\mathbf{B}(t))$ is the number of chain conformations subject to the constraints determined by the R-basin vector $\mathbf{B}(t)$. The possibility of subordinating or entraining the folding process to the coarse-grained stochastic dynamics hinges on an adiabatic scheme whereby intra-R-basin equilibration occurs faster that inter-basin transition.[15,16] Since we adopt a Monte Carlo scheme, we get: $p(t)=\exp[-\Delta\Delta G(t)/ k_B T]$ if $\Delta\Delta G(t)>0$ at T=303K and p(t)=1 otherwise. If at time t, the coarse move $\mathbf{B}(t)=\mathbf{B}\rightarrow\mathbf{B'}$ is rejected by the Monte Carlo procedure, the system remains in topological state **B** for another 1ns ($\mathbf{B}(t+\tau)=\mathbf{B}(t)=\mathbf{B}$) during which it undergoes a second round of equilibration with the solvent.

The AMBER package is adopted to equilibrate with the solvent (Supplementary Material)[19] with the constraint that (Φ, Ψ)-coordinates remain within the R-basins that define the coarse state. Within the AMBER package, the energy stored in the orthogonal

non-Debye polarization, or, equivalently, in the distortion of water structure, is not included in the thermodynamic potential ΔG.

To test the consequences of such common omission and the steering power of the MED principle, we generated 8 folding MC trajectories for an autonomously folding protein within an NPT (isothermal/isobaric, T=303K) ensemble. The first 4 trajectories were generated with coarse states equilibrated and transitioned using the standard potential ΔG, while the remaining 4 trajectories contained coarse states equilibrated and transitioned using the potential $\Delta G_{tot}=\Delta G+\Delta G_{\phi}$ that incorporates the interfacial contribution. Each trajectory consists of $5.2x10^4$ coarse moves, with each coarse state or chain topology generated by the underlying stochastic process. Two representative trajectories are reported in this work, the first reported (Figs. 4, 5) adopting the potential ΔG, and the second (Figs. 6-8), adopting the potential ΔG_{tot}. All trajectories in each group reproduce the destiny structures reported in this work to within 1Å RMSD, as well as the free energy and interfacial free energy patterns hereby reported. In other words, the results are robust in the sense that the folding trajectories in the absence of the interfacial term consistently generate structures in the same topological class, and the same can be stated for trajectories that include the interfacial term. Due to our computational limitations, mitigated by the underlying coarse grained dynamics, we chose a relatively short (N=57) protein chain capable of folding autonomously: the thermophilic variant of the B1 domain of protein G from *Streptococcus* (PDB.1GB4).[17] The thermophilic variant was selected over the wild type due to its higher thermal stability. As implied by Fig. 3a, this higher stability should minimize the interfacial free energy cost beyond wild-type levels and hence should provide a better testing ground to validate the MED principle.

Fig. 4 reveals that when the interfacial term ΔG_ϕ is excluded from the potential that controls the underlying stochastic process, the chain reaches a free energy minimum in about 27μs but contains an interfacial free energy that is approximately 14kJ/mol above the random coil value (ΔG_ϕ=14kJ/mol). The interfacial free energy has not been minimized along the trajectory but instead reaches its maximum at 27μs. As expected, the destiny steady state has an equilibrated conformation (Fig. 5a) that is topologically different from the native state of the protein (Fig. 5b). This dynamic behavior together with the incorrect destiny structure clearly suggest the need to incorporate the interfacial term ΔG_ϕ into the potential.

A representative folding trajectory incorporating the interfacial free energy in coarse grained transitions and structure equilibration is reported in Figs. 6-8. Thus, $\Delta U_\phi(t)$ was calculated using Eq. 8 as the difference in interfacial energy between equilibrated conformations within the ensembles **B**(t) and **B**(0)=random coil ensemble, while $\Delta S_{tot}=\Delta S+\Delta S_\phi$. This time, the trajectory converges at about 27μs to a destiny steady state (structure C, Fig. 6) with a relative free energy ΔG_ϕ that is not the global minimum. In fact, the latter is achieved at 20μs (structure B, Figure 6), while another minimum is achieved at 10μs (structure A, Figure 6).

Strikingly, *although the destiny structure is not the global free energy minimum, it is the structure that realizes the minimum in interfacial free energy* (ΔG_ϕ=-10kJ/mol approximately), *as shown in Fig. 7. It is also the correct structure, topologically equivalent to the native fold* (compare structure C in Fig. 6 with the native structure in Fig. 5b obtained from PDB.1GB4), *with a highly similar contact matrix (Fig. 8) and RMSD=1.32Å.* Furthermore, as shown in Fig. 7, leaving aside fluctuations, the interfacial

free energy is consistently decreasing throughout the simulation, implying that the MED principle has been operative. The destiny structure that minimizes interfacial free energy (Figs. 6 (C), and 8a) has a significantly higher number of tertiary (nonlocal) contacts (32, as shown in Fig. 8a) compared with those that represent local minima in ΔG, shown in Figs. 5 and 6(A,B), with 21, 17 and 12, respectively. This observation suggests a structural signature of the MED principle and prompts further work.

The results reported in Figs. 6-8, jointly with the fact that the destiny steady state is topologically and geometrically very close to the native fold (PDB.1GB4), imply that protein folding seeks to minimize interfacial tension or the disruption of the water hydrogen-bond matrix, in accord with the MED principle.

VI. CONCLUDING REMARKS

The need for a nanoscale theory of water dielectrics has become pressing ever since people became aware that the discrete nature of biological aqueous interfaces defies the inherently continuous laws of electrostatics, or takes them beyond the limits of their applicability. Reconciling the nanoscale hydrogen-bond structure of water with continuous dielectric equations has become a challenge. When dealing with nanoscale confinement, where water is deprived of hydrogen bonding opportunities, this challenge must be inevitably met. This work addresses this challenge, deriving and validating a partial differential equation that governs the episteric distortions of the water hydrogen-bond matrix under nanoscale confinement. In the particular case where confinement occurs at the protein-water interface, the main claim of the work is that the interfacial

energy stored in the episteric distortion of water structure correlates with the energy stored in the polarization orthogonal to the electrostatic field of the protein.

As shown in section III, there is a significant free-energy cost associated with the episteric distortion of the water matrix, and this energetic cost is responsible for partially destabilizing the native fold of proteins. Thus, it is natural to expect that proteins, that are capable of changing their interface with water through internal conformational change, would fold operationally subject to a principle of minimal episteric distortion (MED). This is indeed the case as shown in section V. Our results uphold the MED principle as a determinant of the protein folding process. The interpretation of protein folding as an interfacial tension phenomenon was anticipated by Oktay Sinanoglu and the author in 1985,[18] although the technology was not in place at the time to properly compute the reversible work needed to span the protein-water interface.

ACKNOWLEDGMENTS

This research was supported by CONICET, the National Research Council of Argentina. The author is indebted to Profs. Ridgway Scott and Sze-Bi Hsu for helpful discussions and to Drs. Andrés Colubri and Jianping Chen for their help with the computations.

REFERENCES

1. P. Wernet, D. Nordlund, U. Bergmann, M. Cavalleri, M. Odelius, H. Ogasawara, L. Näslund, T. K. Hirsch, L. Ojamäe, P. Glatzel, L. G. Pettersson and A. Nilsson, Science **304**, 995 (2004).

2. T. Head-Gordon and G. Hura, Chem. Rev. **102**, 2651 (2002).

3. Y. K. Cheng and P. Rossky, Nature **392**, 696 (1998).

4. A. Fernández, J. Chem. Phys. **137**, 231101 (2012).

5. A. Fernández, Phys. Rev. Lett. **108**, 188102 (2012).

6. N. Giovambattista, C. F. Lopez, P. Rossky and P. Debenedetti, Proc. Natl. Acad. Sci. U.S.A. **105**, 2274 (2008).

7. P. Debye, Polar Molecules (Dover Publications, New York, 1929).

8. E. G. Strekalova, M. G. Mazza, H. E. Stanley, and G. Franzese, Phys. Rev. Lett. **106**, 145701 (2011).

9. S. Tanizaki and F. Feig, J. Chem. Phys. **122**, 124706 (2005).

10. H. E. Stanley, S. V. Buldyrev, P. Kumar, F. Mallamace, M. G. Mazza, K. Stokely, L. Xu, and G. Franzese, J. Non-Cryst. Solids **357**, 629 (2011).

11. P. Kumar, S. Han, and H. E. Stanley, J. Phys.: Condens. Matter **21**, 504108 (2009).

12. S. Accordino, D. C. Malaspina, J. A. Rodriguez Fris and G. A. Appignanesi, Phys. Rev. Lett. **106**, 29801 (2011).

13. M. Feig, W. Im and C. L. Brooks III, J. Chem. Phys. **120**, 903 (2004).

14. F. Despa, Ann. N. Y. Acad. Sci. **1066**, 1 (2006).

15. A. Fernández, J. Chem. Phys. **114**, 2489 (2001).

16. A. Fernández, *Transformative Concepts for Drug Design: Target Wrapping*. Chapter 3. Springer-Verlag, Berlin (2010).

17. S. M. Malakauskas and S. L. Mayo, Nat. Struct. Biol. **5**, 470 (1998).

18. O. Sinanoglu and A. Fernández, Biophys. Chem. **21**, 157 (1985).

19. See supplementary material at _____ for details on the application of Gauss' divergence theorem to derive Eq. 7, and on molecular dynamics simulations.

Figure Legends

Figure 1. Schematic depiction of the aqueous interface with boundary conditions that become constraints in determining the coarse-grained descriptor ϕ=4-g of water structure. The interface is defined by the water-smeared envelope $\partial\Omega$ of the solute. It is assumed that the solute surface has a topography endowed with nanoscale detail that may perturb the structure of interfacial water relative to bulk-like patterns. We get ϕ=4 (no water) in the "core" volume Ω_0 at distance d=2r=8Å from each point on $\partial\Omega$, while ϕ=0 for points at distance larger than 3d=24Å from $\partial\Omega$. The latter condition holds since 3d >> 4 water layers (~13Å) from the interface and hence in this region, water structure is assumed to have recovered its bulk-like pattern. The regions where the structure of interfacial water is relatively undistorted show an alignment between episteric polarization **P** and the electrostatic field **E**, whereas regions of high structural distortion likely depart from the linear dielectrics picture, as reflected by a lack of alignment between the fields **P** and **E**.

Figure 2. a. Local deviation from **E**-aligned polarization measured as $\Gamma^{\#}/\Gamma$ and plotted against the structural function ϕ=4-g. The quotient $\Gamma^{\#}/\Gamma$ is evaluated at protein/water interfaces as a time average over an interval beyond protein structure/solvent equilibration. To determine $\Gamma^{\#}/\Gamma$, the episteric polarization **P**=**P(r)** for 9 soluble natural proteins with structures reported in the Protein Data Bank (PDB, Supplementary Material, Table S1)[19] is computed and averaged for each position in space along a thermalization molecular dynamics trajectory (Supplementary Material).[19] The region spanning a distance of 3d=24Å from $\partial\Omega$ (cf. Fig. 1) is exhaustively interrogated by covering it with disjoint spheres of radius 4Å centered at points $\mathbf{r}_n$ (n=1, 2,…) to

determine the set of water-structure values $\phi(\mathbf{r}_n)$. The trend line and correlation coefficient were obtained by linear regression. **b.** Behavior of $\phi=\phi(x)$ relative to the distance x to an interface. The interface is assumed nonpolar, consisting of a concave region of fixed curvature radius θ, with x=0=center of curvature. The flat surface represents the macroscopic limit $\theta>>1$nm, and ϕ-values are shown in the grey plot. Other perturbations were obtained for $\theta=3$Å (thin black plot), and $\theta=2.5$Å (thick black plot).

Figure 3. a. Anticorrelation between the free-energy change (ΔG) for thermal denaturation of soluble monomeric proteins (Supplementary Material, Table S1)[19] and the reversible work (free energy increment ΔG_ϕ) performed to span their aqueous interfaces. The latter thermodynamic parameter is computed using Eq. 8. The trend line and correlation coefficient were obtained by linear regression. The result suggests that protein destabilization is commensurate with the thermodynamic cost of creating the interface and inspires the principle of minimal episteric distortion (MED) that serves as guidance for soluble proteins that seek their native fold. **b**. Correlation between $W^{\#}$ (filled squares) and ΔU_ϕ, both normalized by solvent-accessible surface area, for the 9 proteins with PDB representation described in Table S1. The proteins are distributed along the abscissas in decreasing order of denaturation free energy (cf. Fig. 3a). The normalized $W^{\|}$-values (empty squares) are also plotted. The trend line and correlation coefficient were obtained by linear regression.

Figure 4. Folding trajectory steered by an underlying coarse-grained stochastic process consisting of $5.2\text{x}10^4$ coarse moves representing transitions and equilibrations of

topological states of the chain for the thermophilic variant of the B1 domain of protein G,[17] an autonomous folder with native fold reported in PDB entry 1GB4. The folding trajectory was generated adopting ΔG as potential determinant of coarse moves and equilibration. **a.** Time-dependent behavior of the free energy ΔG relative to the random coil ensemble. **b.** Time-dependent behavior of the interfacial free energy ΔG_ϕ.

Figure 5. a. Ribbon representation of the destiny steady state conformation for the simulation described in Figure 4. **b.** Native fold in ribbon representation obtained from the structural coordinates reported in PDB.1GB4.

Figure 6. Folding trajectory consisting of 5.2×10^4 coarse moves representing transitions and equilibrations of topological states of the chain for the thermophilic variant of the B1 domain of protein G. The folding trajectory was generated adopting the thermodynamic potential $\Delta G_{tot} = \Delta G_\phi + \Delta G_\phi$ as determinant of coarse moves and equilibration within coarse states. The trajectory is described by the time-dependent behavior of the free energy ΔG relative to the random coil initial state. Three equilibrated conformations at 10, 20 and 50μs are shown in ribbon representation and denoted A, B, C, respectively. The steady-state conformation C is not the global minimum in free energy.

Figure 7. Time-dependent behavior of the relative interfacial free energy ΔG_ϕ for the trajectory described in Fig. 6. The steady-state conformation C from Fig. 6 actually realizes the minimum of ΔG_ϕ.

Figure 8. Contact matrices associated with the equilibrated destiny conformation generated by the folding trajectory described in Figs. 6, 7 (**a**) and with the native fold shown in ribbon representation in Fig. 5b (**b**), respectively. An (i,j) entry in the matrix is filled in black if the minimum Euclidean distance $d_{min}(i,j)$ between atoms in residues i and j is ≤4Å, grey if 4Å<$d_{min}(i,j)$ ≤6Å, with the upper bound being the effective cut-off for long-range interactions,[16] and white if $d_{min}(i,j)$ >6Å. The two matrices reveal the same topological pattern of antiparallel and parallel β-sheets and α-helix.

FIGURE 1

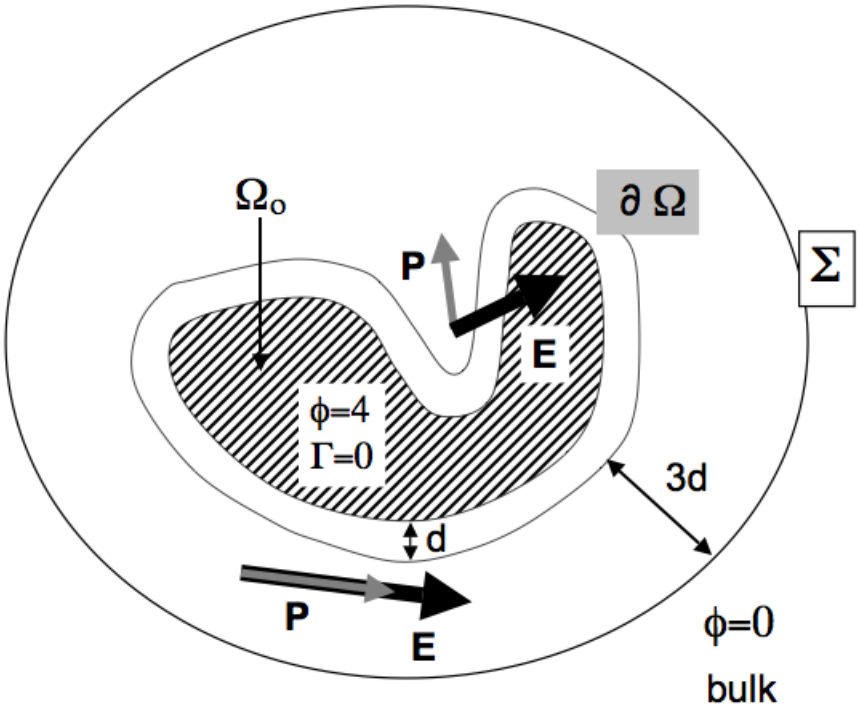

FIGURE 2a

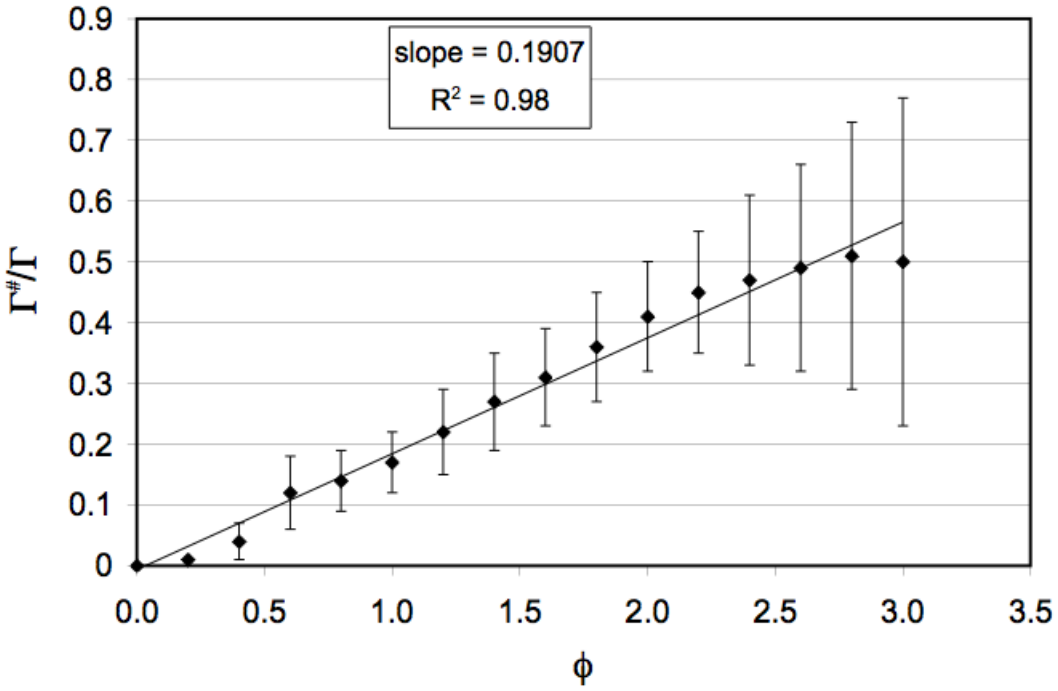
slope = 0.1907
R² = 0.98
Γ#/Γ
ϕ
0.9
0.8
0.7
0.6
0.5
0.4
0.3
0.2
0.1
0
0.0
0.5
1.0
1.5
2.0
2.5
3.0
3.5

FIGURE 2b

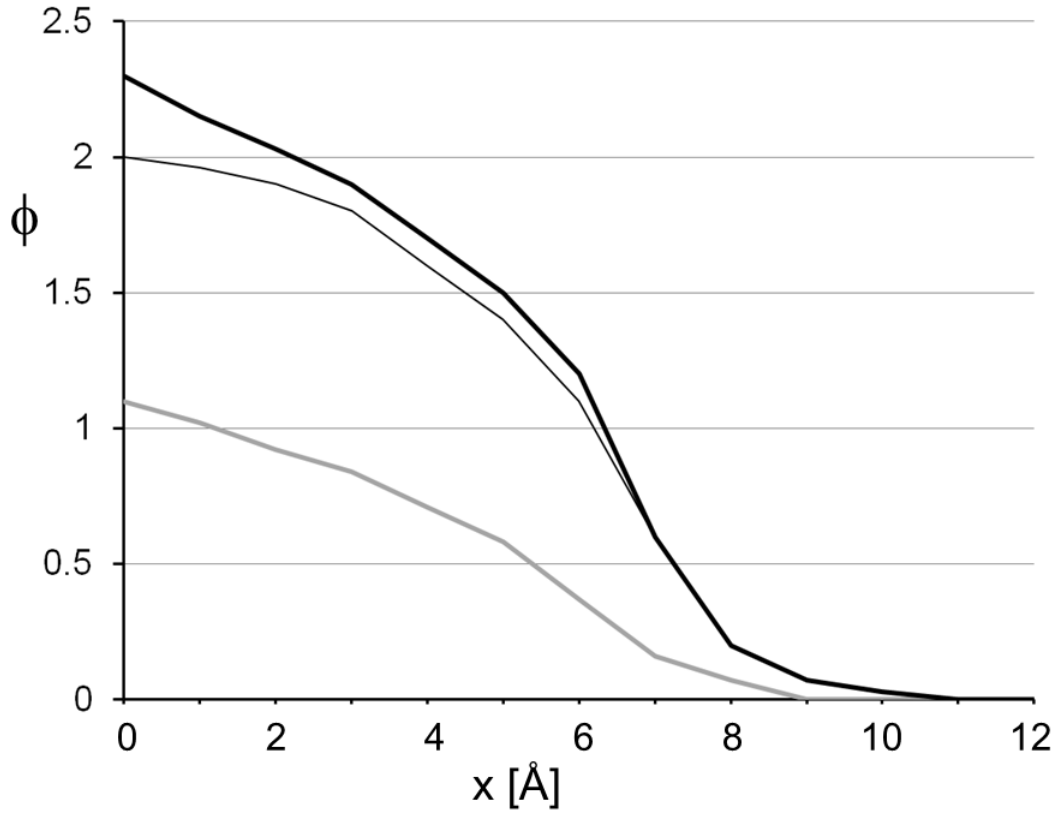

FIGURE 3a

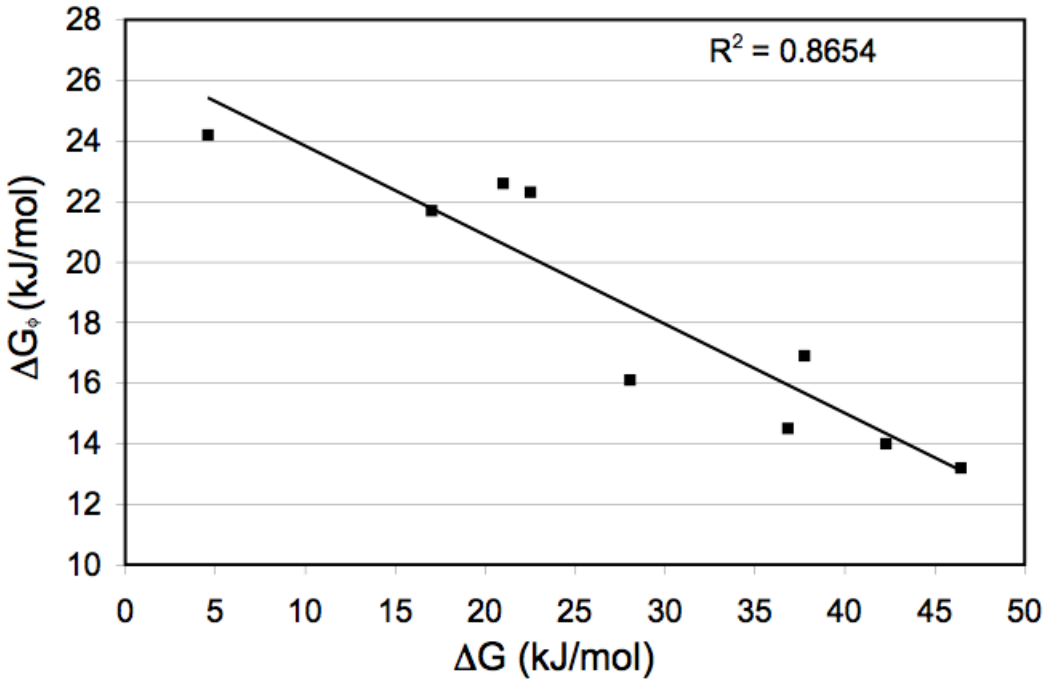
R^2 = 0.8654
ΔG_ϕ (kJ/mol)
28
26
24
22
20
18
16
14
12
10
0
5
10
15
20
25
30
35
40
45
50
ΔG (kJ/mol)

FIGURE 3b

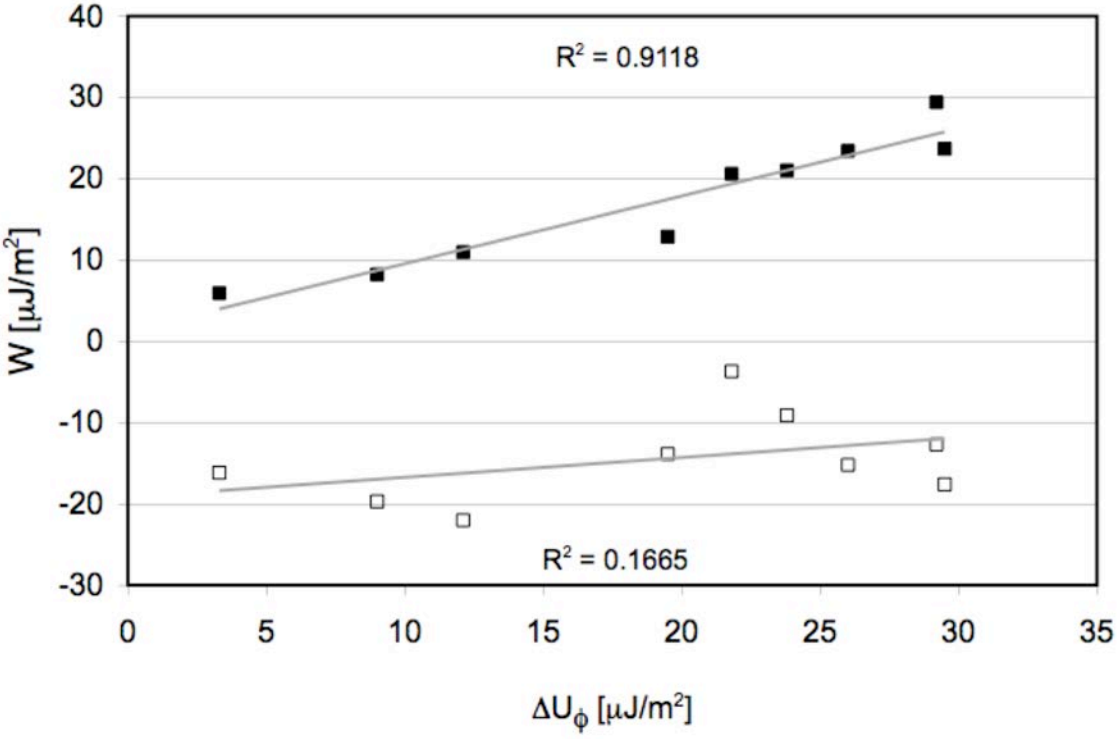
R² = 0.9118
R² = 0.1665
W [μJ/m²]
ΔU_φ [μJ/m²]
40
30
20
10
0
-10
-20
-30
0
5
10
15
20
25
30
35

FIGURE 4

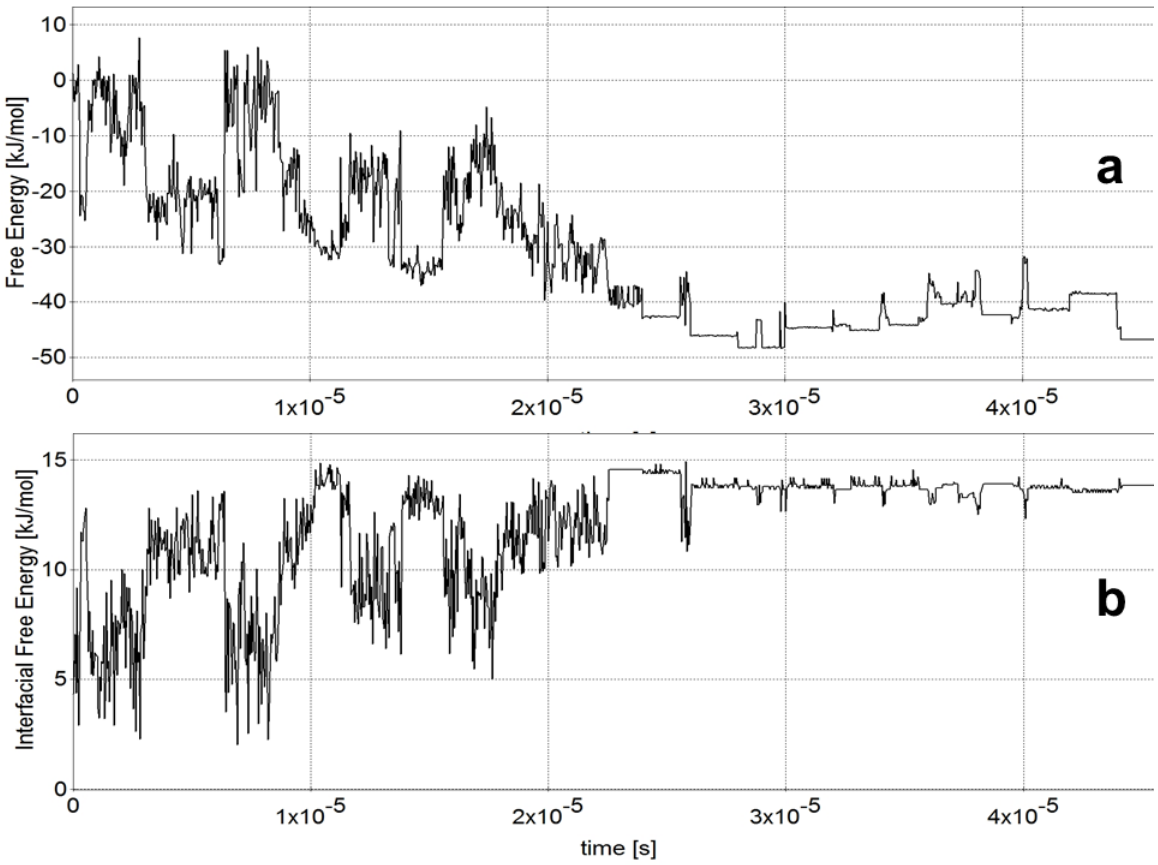
Free Energy [kJ/mol]
10
0
-10
-20
-30
-40
-50
0
1x10^-5
2x10^-5
3x10^-5
4x10^-5
a
Interfacial Free Energy [kJ/mol]
15
10
5
0
0
1x10^-5
2x10^-5
3x10^-5
4x10^-5
time [s]
b

FIGURE 5

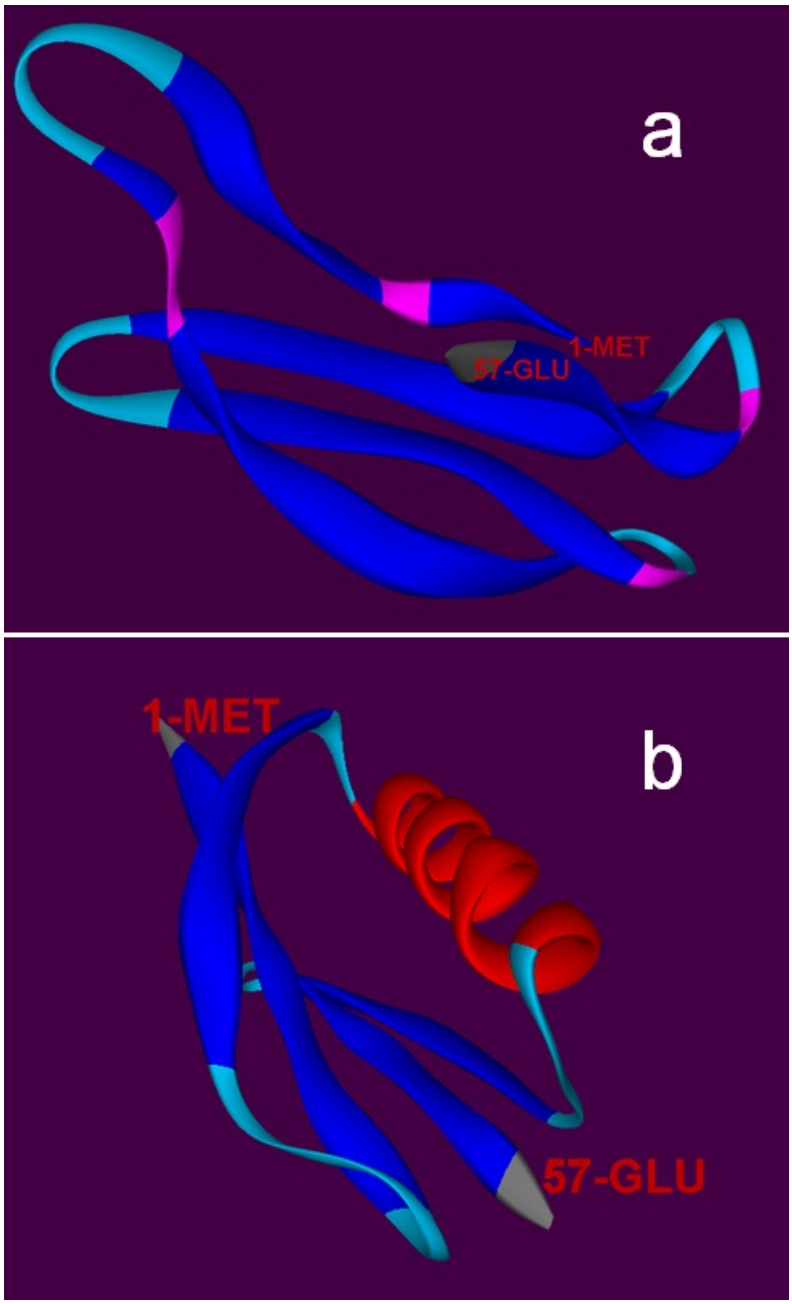

FIGURE 6

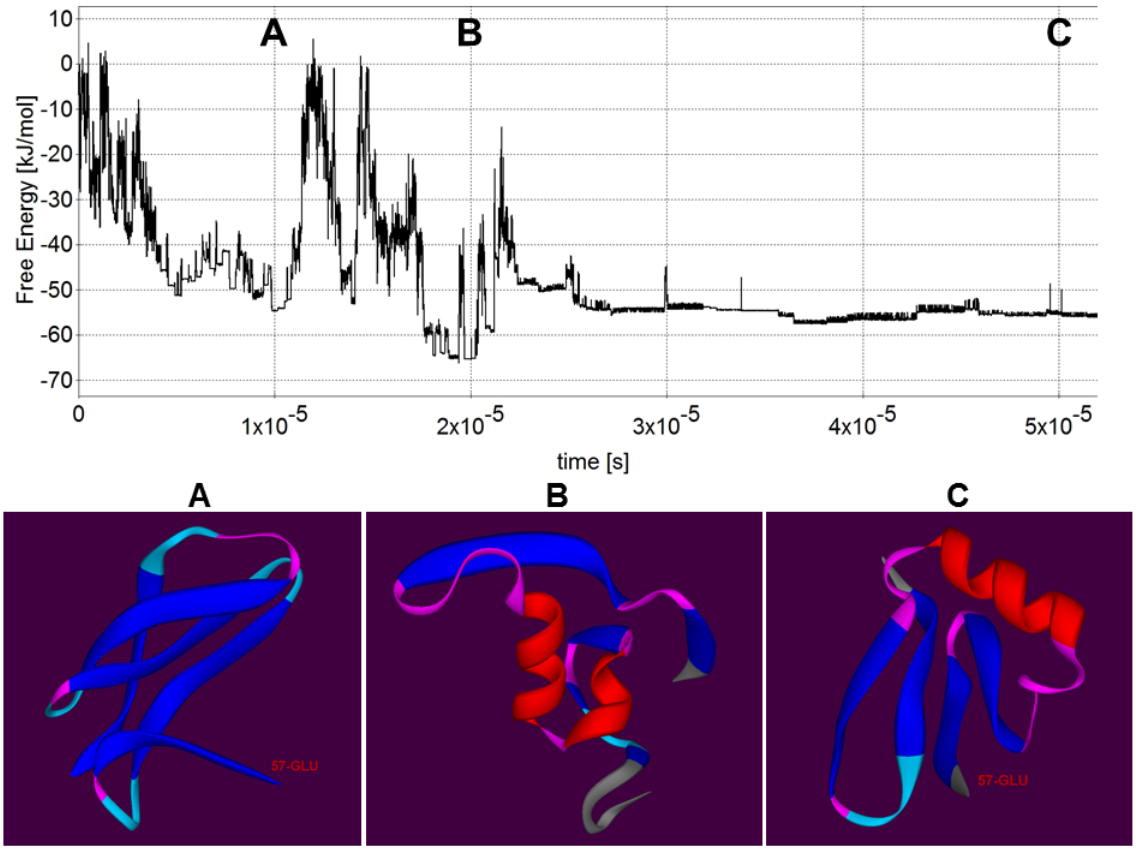

FIGURE 7

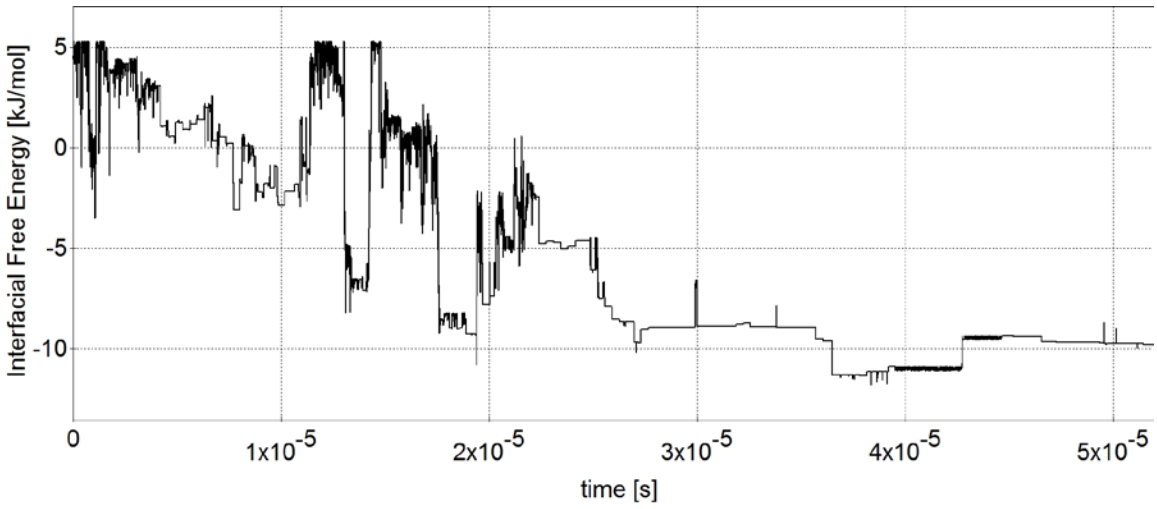

FIGURE 8